MODELING THE RADIAL VELOCITIES AND PROPER MOTIONS OF HERBIG-HARO OBJECTS

A. C. Raga,[1] P. F. Velázquez,[1] J. Cantó,[2] and E. Masciadri[2]

RESUMEN

Este artículo discute los diferentes métodos que han sido usados para modelar la emisión de objetos Herbig-Haro (HH). Aunque simulaciones axisimétricas y 3D han sido realizadas para modelar objetos específicos, la mayor parte de las comparaciones entre teoría y observaciones han estado basadas en el uso de descripciones analíticas sencillas de la estructura cinemática de jets. Describimos estos modelos analíticos y presentamos algunas nuevas posibilidades.

ABSTRACT

This paper discusses the different approaches that have been used for modeling the emission of Herbig-Haro (HH) objects. Even though axisymmetric or 3D simulations have been carried out for modeling specific objects, most comparisons carried out between theory and observations have been based on the use of simple, analytic descriptions of the kinematical structure of jets. These analytic models are summarized and some new possibilities are discussed.

Key Words: **HYDRODYNAMICS — ISM: JETS AND OUTFLOWS — STARS: PRE-MAIN-SEQUENCE**

1. INTRODUCTION

The first comparisons carried out between the observed emission line spectrum of HH objects and theoretical models were based on plane-parallel, stationary shock models (Dopita 1978; Raymond 1979). This type of modeling has survived the passage of the years, and is still alive and well among us (e.g., Hartigan, Morse, & Raymond 1994; Lavalley-Fouquet, Cabrit, & Dougados 2000), with an extensive literature covering comparisons with many HH objects.

These models were extended to compute "3/2-D" bowshocks, in which the emission of a parameterized bowshock shape is approximated with a sequence of 1D shocks of appropriate shock velocities. This approach was pioneered by Hartmann & Raymond (1984), and has been used in order to model the line ratios and line profiles of many HH objects (e.g., Hartigan, Raymond, & Hartmann 1987; Solf, Böhm, & Raga 1986). Again, this dinosaur is still roaming among us (the most recent example appears to be the work of Froebrich, Smith, & Eislöffel 2002).

More advanced models based on 2D or 3D numerical simulations have been computed for specific HH objects, but the number of modeled objects is quite small: HH 1 (Raga et al. 1988), HH 34 (Raga & Noriega-Crespo 1998; Cabrit & Raga 2000; de Gou-

veia dal Pino 2001), HH 111 (Völker et al. 1999; Masciadri et al. 2002), the DG Tauri microjet (Raga et al. 2001), HH 505 (Masciadri & Raga 2001) and HH 110 (Raga & Cantó 1995; de Gouveia dal Pino 1999). Some other numerical simulations have been compared with HH flows, but mostly without taking particular care to try to reproduce the observed structures in detail.

However, most comparisons between observations of HH objects and models have been based on simple, analytic expressions relating the line profiles produced by 3/2-D bowshocks to the flow parameters. These analytic expressions were derived by Hartigan et al. (1987), and are summarized in § 2.

A decade later, similar analytic expressions were derived for the proper motions of condensations in a bowshock flow by Raga et al. (1997), who used this model to derive the flow parameters from the observed proper motions of condensations in HH bowshocks. This technique is described in § 3.

Very recently, papers have been published with very detailed proper motions of HH objects obtained from *HST* images (Hartigan et al. 2001; Reipurth et al. 2002). We find that these proper motions allow a more detailed reconstruction of the properties of the flow than was possible from the two techniques described above. The new possibilities are discussed in § 4.

[1]Instituto de Ciencias Nucleares, UNAM, México.
[2]Instituto de Astronomía, UNAM, México.

2. FLOW PARAMETERS DERIVED FROM THE OBSERVED LINE PROFILES

Hartigan et al. (1987) demonstrated that the maximum ($v_{\mathrm{r,max}}$) and minimum ($v_{\mathrm{r,min}}$) radial velocities measured in a line profile generated by a 3/2-D bowshock can be used to derive the bowshock velocity v_{bs} and the orientation angle ϕ with respect to the plane of the sky. The relations that give these parameters are:

$$v_{\mathrm{bs}} = v_{\mathrm{r,max}} - v_{\mathrm{r,min}} \,, \qquad (1)$$

$$\phi = \sin^{-1}\left[\frac{v_{\mathrm{r,max}} + v_{\mathrm{r,min}}}{v_{\mathrm{r,max}} - v_{\mathrm{r,min}} + 2\,v_{\mathrm{f}}}\right] \,, \qquad (2)$$

where v_{bs} is the velocity of the bowshock relative to the downstream medium and ϕ is the angle between the outflow axis and the plane of the sky (positive angles indicating flows directed away from the observer). Also, it has been assumed that the environment into which the bowshock is moving, has a non-zero velocity v_{f} directed away from the outflow source. This "environmental velocity" is assumed to be homogeneous (i.e., that it has the same value for all positions along the bowshock surface), and is introduced in order to model an outflow event which is moving into material which was previously ejected from the source.

Clearly, the introduction of v_{f} allows a range of possible values of v_{bs} and ϕ for a given set of observed $v_{\mathrm{r,max}}$ and $v_{\mathrm{r,min}}$. This indeterminacy can be removed through a more detailed modeling of the line profiles using predictions from numerical, 3/2-D bowshock models (Hartigan et al. 1987). Another possibility for doing this is to analyze the proper motions observed for the bowshock flow. This is described in the following section.

We should note that there are some subtleties in the determination of $v_{\mathrm{r,max}}$ and $v_{\mathrm{r,min}}$. One point is that they have to be corrected for the systemic velocity (i.e., $v_{\mathrm{r}} = 0$ has to correspond to the radial velocity of the outflow source). The second, more important point is that it is not completely clear which are the maximum and minimum radial velocities in an observed line profile. For example, emission farther away from the line centre is generally detected in higher signal-to-noise data. There is no solution to this lack of a clear observational definition of $v_{\mathrm{r,max}}$ and $v_{\mathrm{r,min}}$ (for some suggestions, see Hartigan et al. 1987).

3. FLOW PARAMETERS DERIVED FROM THE OBSERVED PROPER MOTIONS

Raga et al. (1997) carried out an analysis similar to the one of Hartigan et al. (1987), but for
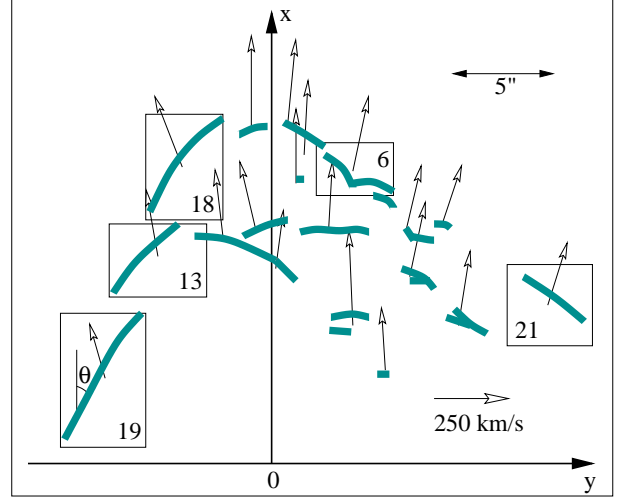
Fig. 1. Schematic diagram showing the filamentary structure observed in Hα *HST* images of HH 34S and the proper motions derived by Reipurth et al. (2002). The *x*-axis approximately coincides with the outflow axis. We have chosen 5 of the cross-correlation boxes of Reipurth et al. (2002), which lie along the edge of the bowshock and which include filamentary structures with well defined orientations (the boxes are numbered 6, 13, 18, 19, and 21).

the proper motions of condensations participating in a 3/2-D bowshock flow. The proper motions have more information than the radial velocities, since they have two independent components (parallel and perpendicular to the outflow axis).

Raga et al. (1997) show that the maximum and minimum proper motion velocities perpendicular to the outflow axis ($v_{\perp,\mathrm{max}}$ and $v_{\perp,\mathrm{min}}$, respectively) satisfy the relation:

$$v_{\mathrm{bs}} = v_{\perp,\mathrm{max}} - v_{\perp,\mathrm{min}} \,, \qquad (3)$$

and that the maximum and minimum proper motion velocities along to the outflow axis *for condensations on the projected rim of the bowshock* ($v_{\parallel,\mathrm{max}}$ and $v_{\parallel,\mathrm{min}}$, respectively) satisfy the relation:

$$v_{\mathrm{bs}}\cos\phi = v_{\parallel,\mathrm{max}} - v_{\parallel,\mathrm{min}} \,, \qquad (4)$$

so that the angle between the outflow axis and the plane of the sky can be found from the relation:

$$\phi = \cos^{-1}\left[\frac{v_{\parallel,\mathrm{max}} - v_{\parallel,\mathrm{min}}}{v_{\perp,\mathrm{max}} - v_{\perp,\mathrm{min}}}\right] \,. \qquad (5)$$

The velocity v_{f} of the environment immediately downstream of the bowshock can be determined from the relation:

$$v_{\mathrm{f}} = \frac{v_{\parallel,\mathrm{min}}}{\cos\phi} \,. \qquad (6)$$
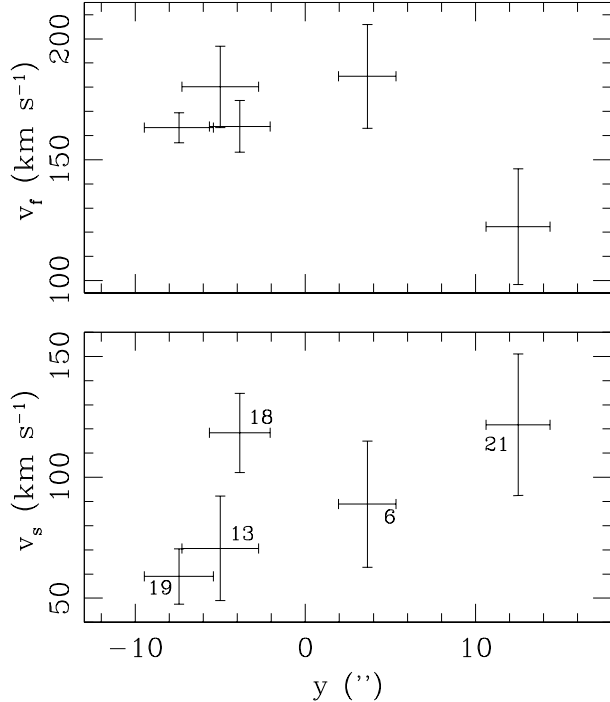
Fig. 2. Flow velocity ahead of HH 34S (top) and shock velocity (bottom) derived for the regions within the boxes shown in Figure 1 (also see Reipurth et al. 2002). The horizontal bars give the location and size of the respective cross-correlation boxes. The vertical bars give the errors in the derived velocities. These errors are dominated by the uncertainty in the orientation θ of the filaments, which was estimated to have a $\Delta\theta \approx 1°$ value.

In this way, the three flow parameters v_{bs}, ϕ and v_{f} can be determined from the observed maximum and minimum proper motion velocities along and across the outflow axis.

Curiel et al. (1997) applied this method to their proper motions of HH 32 (which were derived from a combination of *HST* images and previous, ground based adaptive optics observations), and derived flow parameters for this object which were basically identical to previous results obtained from analyses of line profiles (Solf et al. 1986; Hartigan et al. 1987). Raga et al. (1997) tried to apply this method to other objects (HH 1 and HH 34) and also found results which are consistent with the radial velocity data.

4. NEW POSSIBILITIES

The recently published *HST* proper motions of HH 1/2 (Hartigan et al. 2001) and HH 34 (Reipurth et al. 2002) show much finer detail than any previous measurements and open new possibilities for the kind of analysis described in the previous section. As an example, in Figure 1 we show a schematic

diagram with the filamentary structure seen in the Hα *HST* images of HH 34S and the proper motions determined by Reipurth et al. (2002).

From this figure, it is completely clear that the proper motions of condensations on the projected rim of the bowshock do not point in a direction normal to the bowshock surface. All of the proper motions point somewhere in between the shock normal and the outflow direction.

Because of the fact that a shock pushes material only in the direction of the shock normal, the components of the proper motion velocities tangential to the shock surface have to be present in the pre-shock flow. Therefore, the component tangential to the bowshock of the velocity of the material immediately ahead of the bowshock has to be equal to $v_x \cos\theta - |v_y| \sin\theta$, where v_x and v_y are the components of the proper motion velocity along and across the outflow axis, and θ is the angle between the outflow axis and the local direction of the surface of the bowshock (see Fig. 1).

If we assume that the upstream material moves in a direction parallel to the outflow axis, we can then de-project the tangential component to obtain its full velocity:

$$v_{\mathrm{f}} = v_x - |v_y| \tan\theta \,. \qquad (7)$$

It is also then possible to compute the shock velocity as the difference between the components along the shock normal of the proper motion velocity and the velocity of the material directly ahead of the bowshock:

$$v_{\mathrm{s}} = v_x \sin\theta + |v_y| \cos\theta - v_{\mathrm{f}} \sin\theta \,. \qquad (8)$$

Equations (7) and (8) can be used to determine the shock velocity and the velocity of the material ahead of the bowshock for all of the filamentary condensations along the leading edge of the bowshock. In this way, the assumption of a position-independent v_{f} (which was made in §§ 2 and 3) can now be relaxed. The results obtained from this exercise are shown in Figure 2.

This figure shows that even though the errors are rather large, it is possible to reconstruct the profiles of the shock velocity v_{s} and the downstream flow velocity v_{f} along the leading edge of HH 34S. We find that the shock velocities range from 60 to 120 km s^{-1}, which is in principle consistent with the high excitation nature of the object. Interestingly, we find that the downstream flow velocity v_{f} has values ranging from 120 up to 185 km s^{-1}, with the higher velocities close to the symmetry axis,

and lower velocities farther away along the bowshock wings.

If we take this result at face value, it implies that HH 34S is moving into a region moving away from the outflow source with a velocity of ~ 180 km s^{-1}. As is clear from Fig. 2, this high velocity flow extends to $\sim 10''$ to each side of the outflow axis, and has a strongly decreasing velocity for larger distances from the axis.

The nature of this upstream flow is not completely clear. Two explanations are possible:

- HH 34S could be moving into a very wide, high velocity wake left behind by previous outflow events,

- the high velocity material upstream of HH 34S could be associated with a broader outflow (ejected from the source) within which is travelling the optically observed HH 34 jet.

Clearly, both possibilities are intriguing, and deserve further study.

We should note that for deriving the above results, we have assumed that the outflow axis lies on the plane of the sky. As previous determinations of the orientation of the HH 34 outflow indicate that its axis lies at approximately $\phi = -30°$ from the plane of the sky, our $\phi \approx 0$ assumption will not introduce large errors in the determined velocities.

5. CONCLUSIONS

The most popular way of deriving flow parameters for HH objects has been to use the kinematical 3/2-D bowshock relations derived by Hartigan et al. (1987), which involve the maximum and minimum radial velocities derived from observed line profiles. We have described these relations, and have also discussed the similar relations derived by Raga et al. (1997) for the proper motion velocities of a bowshock.

Interestingly, the recently published *HST* proper motions of HH objects (Hartigan et al. 2001; Reipurth et al. 2002) allow a more detailed analysis of the properties of bowshock flows. We show that from the observations of HH 34S of Reipurth et al. (2002) it is possible to derive the position-dependent velocity v_f of the flow directly ahead of the bowshock.

From this, we see that the more detailed observations (derived from high angular resolution observations) that are now appearing are likely to give new life to simple, analytic models, which relate the observed parameters (i.e., proper motions and/or radial velocities) to the propeties of the flow. Such models should be useful to guide more detailed modeling based on full numerical simulations of the outflows.

REFERENCES

Cabrit, S., & Raga, A. C. 2000, A&A, 354, 667
Curiel, S., Raga, A. C., Raymond, J. C., Noriega-Crespo, A., & Cantó, J. 1997, AJ, 114, 2736
de Gouveia dal Pino, E. 1999, ApJ, 526, 862
_____. 2001, ApJ, 551, 347
Dopita, M. A. 1978, ApJS, 37, 117
Froebrich, D., Smith, M. D., & Eislöffel, J. 2002, A&A, 385, 239
Hartigan, P., Morse, J. A., & Raymond, J. C. 1994, ApJ, 436, 125
Hartigan, P., Morse, J. A., Reipurth, B., Heathcote, S., & Bally, J. 2001, ApJ, 559, L157
Hartigan, P., Raymond, J. C., & Hartmann, L. 1987, ApJ, 316, 323
Hartmann, L., & Raymond, J. C. 1984, ApJ, 276, 560
Lavalley-Fouquet, C., Cabrit, S., & Dougados, C. 2000, A&A, 356, L41
Masciadri, E., & Raga, A. C. 2001, AJ, 121, 408
Masciadri, E., Velázquez, P. F., Raga, A. C., Cantó, J., & Noriega-Crespo, A. 2002, ApJ, in press.
Raga, A. C., Cabrit, S., Dougados, C., & Lavalley, C. 2001, A&A, 367, 959
Raga, A. C., & Cantó, J. 1995, RevMexAA, 31, 51
Raga, A. C., Cantó, J., Curiel, S., Noriega-Crespo, A., & Raymond, J. C. 1997, RevMexAA, 33, 157
Raga, A. C., Mateo, M., Böhm, K. H., & Solf, J. 1988, AJ, 95, 1783
Raga, A. C., & Noriega-Crespo, A. 1998, AJ, 116, 2943
Raymond, J. C. 1979, ApJS, 39, 1
Reipurth, B., Heathcote, S., Morse, J., Hartigan, P., & Bally, J. 2002, AJ, 123, 362
Solf, J., Böhm, K. H., & Raga, A. C. 1986, ApJ, 305, 795
Völker, R., Smith, M. D., Suttner, G., & Yorke, H. W. 1999, A&A, 343, 953

A. C. Raga and P. F. Velázquez: Instituto de Ciencias Nucleares, UNAM, Apartado Postal 70-543. 04510 D.F., México (raga@astroscu.unam.mx).
J. Cantó and E. Masciadri: Instituto de Astronomía, UNAM, Apartado Postal 70-264, 04510 D.F., México.